Carbon 157 (2020) 495–505

Contents lists available at ScienceDirect

Carbon

journal homepage: www.elsevier.com/locate/carbon

Evaluation of the textural properties of ultramicroporous carbons using experimental and theoretical methods

D. Grau-Marin [a], J. Silvestre-Albero [a], E.O. Jardim [a], J. Jagiello [b], W.R. Betz [c], L.E. Peña [c, *]

[a] Laboratorio de Materiales Avanzados, Departamento de Química Inorgánica-Instituto Universitario de Materiales, Universidad de Alicante, Alicante, Spain
[b] Micromeritics Instrument Corporation, Norcross, United States
[c] MilliporeSigma, Bellefonte, United States

ARTICLE INFO

Article history:
Received 15 August 2019
Received in revised form
14 October 2019
Accepted 15 October 2019
Available online 18 October 2019

ABSTRACT

Spherical carbon molecular sieves (CMS) have selective adsorptive properties which are suitable for separation and purification of gas mixtures. Precise methods of characterization are needed to understand the performance of CMS in separation processes. To this end, the pore size distribution (PSD) of four carbon molecular sieves were evaluated experimentally using immersion calorimetry and complemented with gas adsorption measurements at cryogenic temperatures for N_2, O_2 and Ar, and at 273 K for CO_2. Theoretical pore size distributions were estimated using two-dimensional non-local Density Functional Theory (2D-NLDFT) models. Calorimetry results showed that B and C samples had a narrow pore size distribution with pores below 0.7 nm. Meanwhile, the pore size distributions calculated from O_2 and Ar adsorption isotherms, gave an apex in the 0.5–0.6 nm region for all the carbons together with a growing development of porosity at around 0.8 nm and above for carbons A and D. The agreement observed between experiments and theory confirmed the validity of the theoretical 2D-NLDFT models to anticipate the PSD. Carbon C with pores exclusively below 0.7 nm separated CO_2 and CH_4 while carbon D with pores in the supermicroporous region separated propane and propylene chromatographically.

1. Introduction

Gas phase separations using porous carbon particles are possible thanks to their tailored textural properties (well-defined pore size window and pore shape) [1]. For the same reason, small scale packed bed systems in analytical applications have made use of porous carbons [2]. Since carbon molecular sieves have been efficient means of separation of molecules with similar molecular weights and chemistries [3], these carbons were effective adsorbents of gas molecules such as CO_2, CH_4, and light hydrocarbons [4]. Driven by environmental concerns, carbon adsorbents have been investigated for CO_2 sequestration to reduce emissions from flue gas in generation plants and biogas digesters [5,6]. Separation of hydrocarbons by pressure swing adsorption (PSA) on carbon molecular sieves (CMS) has been attractive compared to the energy intensive distillation separations such that of ethane and ethene [7], and propane and propylene [8,9]. However, the separation of small molecules with similar kinetic diameters has been a challenge for the current separation systems [8]. The design of adsorbents with tuned textural characteristics and pre-defined surface chemistry aims for more efficient separations. The availability of precise methods of characterization would help to speed up the development of effective adsorbents for difficult separations.

Traditionally, textural properties of nanoporous solids have been evaluated using gas adsorption at cryogenic temperatures (preferentially N_2 adsorption at 77 K and Ar adsorption at 87 K) [10]. These studies showed that Ar at 87 K provides a better description of the pore size distribution compared to N_2 at 77 K due to the absence of a quadrupole moment in Ar that avoids specific interactions with the adsorbent surface. Using Ar isotherms measured at 87 K for the assessment of microporosity was also recommended by the IUPAC Technical Report [11]. In addition to argon, oxygen adsorption isotherms were recently proposed for the PSD analysis [12]. The quadrupole moment of O_2 is less than one-third of the value reported for N_2, which makes O_2 significantly less susceptible to specific surface interaction than N_2. Oxygen has a

* Corresponding author.
E-mail addresses: dgraumarin@gmail.com (D. Grau-Marin), Joaquin.silvestre@ua.es (J. Silvestre-Albero), Erika.jardim@ua.es (E.O. Jardim), Jacek.jagiello@micromeritics.com (J. Jagiello), William.betz@milliporesigma.com (W.R. Betz), leidy.penaduque@milliporesigma.com (L.E. Peña).

https://doi.org/10.1016/j.carbon.2019.10.035

wide liquid-vapor coexistence curve (54–155 K) that allows for using liquid N_2 as a cryogenic bath. Using liquid N_2 instead liquid Ar as a cryogen is practically beneficial due to its lower cost in most parts of the world. CO_2 at 273 K was also proposed as a complementary probe molecule to improve the description of porous networks by specifically evaluating narrow microporosity (pores below 1 nm) in "problematic samples", i.e. samples which are prone to exhibit narrow constrictions [13,14].

Textural parameters such as BET surface area, micropore volume, narrow micropore volume and pore size distribution can be estimated from the gas adsorption isotherms applying first principle theory [15,16]. The 2D-NLDFT characterization method was based on the adsorption models derived from the two-dimensional version of the non-local density functional theory. These models assumed the energetic heterogeneity and roughness of the carbon surface [17], and were more realistic than the standard slit pore model considering the smooth and uniform carbon surface. Using the 2D-NLDFT models for the pore size distributions (PSD) analysis of carbon adsorption data gives results free from known artifacts produced be the standard one-dimensional slit pore model.

PSD obtained after application of the NL-DFT models to gas adsorption isotherms can be complemented in terms of pore size/shape by immersion calorimetry [18]. In the absence of specific interactions at the solid-liquid interface, immersion calorimetry into liquids of different molecular dimensions can also be used to estimate the surface accessibility for the different molecules. Despite the precision of the latest methods to characterize the textural features of an adsorbent; in some cases, the performance of an adsorbent in the separation of a pair cannot be predicted accurately. The underlying uncertainties of static measurements [19,20], theoretical models [21–23], and measurements in dynamic systems [24] might each contribute to differences in separation behaviors. Equilibrium parameters described adsorbent characteristics, but separation was primarily driven by adsorption kinetics [25]. Because the adsorbent particle size, the length to diameter ratio of the column, the pressure and temperature profiles, the gas concentrations could all had an effect on the kinetic parameters; results from one experimental set up could not always be translated to another one. Based on these premises, the objective of this study was to perform the characterization of a series of ultramicroporous carbon molecular sieves combining both experimental and theoretical techniques. The final goal was to predict the CMS separation performance of gas mixtures such as CH_4/CO_2, ethane/ethylene, propane/propylene providing accurate textural characteristics using different probe molecules, including immersion calorimetry, and the theoretical predictions based on NL-DFT methods.

2. Materials and methods

Four polymer-based, 30/80 mesh (180-600μm), experimental, carbons molecular sieves labeled as Carbon A, B, C and D were used in this study and were provided by MilliporeSigma (Bellefonte, USA). Intended for separation of small molecules, the selected carbons were microporous carbons. Preparation of CMS was discussed in a previous work [26].

XPS experiments were performed using a Physical Electronics VersaProbe II instrument equipped with a monochromatic Al kα x-ray source ($h\nu = 1486.7$ eV) and a concentric hemispherical analyzer. Charge neutralization was performed using both low energy electrons (<5 eV) and argon ions. The binding energy axis was calibrated using sputter cleaned Cu (Cu $2p_{3/2} = 932.62$ eV, Cu $3p_{3/2} = 75.1$ eV) and Au foils (Au $4f_{7/2} = 83.96$ eV). Peaks were charge referenced to CH_x band in the carbon 1s spectra at 284.8 eV. Measurements were made at a takeoff angle of 45° with respect to the sample surface plane. This resulted in a typical sampling depth of 3–6 nm (95% of the signal originated from this depth or shallower). Quantification was done using instrumental relative sensitivity factors (RSFs) that accounted for the x-ray cross section and inelastic mean free path of the electrons. The carbon samples were conditioned at 120 °C in a vacuum oven, then stored for 24 h before analysis in vacuum desiccator. Samples were run in triplicate and the confidence intervals calculated as 1.96 times the standard error.

Elemental analysis was performed in a LECO (CHN628, St. Joseph, Mich., USA). The samples were preconditioned at 393K for 16 h in a vacuum oven. The reported values are averages of three measurement replicates. Samples were run in triplicate and the confidence intervals calculated as 1.96 times the standard error.

Pore size distribution of the carbon molecular sieves were evaluated experimentally using immersion calorimetry into liquids of different dimensions. This technique evaluated the enthalpy of immersion of liquids with different kinetic diameters, and indirectly, the pore size accessibility in the carbon samples; as it measured the heat released when a liquid or probe molecule wetted the carbon surface [18]. The experimental pore size distribution was deduced from enthalpy values. The probe molecules used in this study were: dichloromethane (DCM, 0.33 nm), n-hexane (n-hx, 0.43 nm), 2-methyl-pentane (2-MP, 0.5 nm), α-pinene (0.7 nm), and 1,3,5-triisopropylbenzene (TIPB, 0.74×0.85 nm). Immersion calorimetry measurements were performed in a Setaram C80D calorimeter working at 303 K. Before the immersion measurements, samples were outgassed at 523 K overnight under UHV conditions and sealed under vacuum in a glass reactor. The deviation in the calorimetric measurements was lower than 5%.

CO_2 and high resolution N_2 adsorption isotherms were acquired in a home-built manometric equipment designed and constructed by the LMA group (Laboratorio de Materiales Avanzados, University of Alicante, Spain) and currently licensed by Gas to Materials (G2MTech, Alicante, Spain, www.g2mtech.com). N_2 adsorption data were taken at 77 K, while CO_2 data was acquired at 273 K. Before the adsorption experiment, samples were outgassed at 523 K overnight. BET surface area was calculated from the N_2 adsorption data whereas CO_2 data was used to estimate the narrow micropore volume with application of the Dubinin-Radushkevich equation.

The isotherms of N_2, Ar and O_2 were measured using the high-resolution Micromeritics 3Flex instrument equipped with a high-vacuum system, three micropore ports, and three 0.1 Torr pressure transducers. The measurements temperatures were 77 K for N_2 and O_2, and 87 K for Ar. These measurements were analyzed using recently developed 2D-NLDFT models to obtain the PSD characteristics of our carbon samples [12]. N_2 adsorption data were also used to calculate the micro-/meso- and total pore volume.

CO_2 and CH_4 high pressure adsorption isotherms were measured by the LabQMC/Quantachrome Instruments in an iSorbHP1 (Quantachrome Instruments, Bointon Beach, U.S.).

Dynamic separation experiments for CO_2 and CH_4 were carried out in packed chromatographic columns. A, B, C, and D carbons were each packed in 6 ft x 1/8 in stainless steel chromatographic columns. Gas mixtures (4.5%CH_4, 15%CO_2 in N_2) as well as pure components were injected (100 μl) into the columns at 308 K using 20 ml/min He as carrier gas. The pressure in the columns was 0.2–0.3 bar. A thermoconductivity detector TCD was used for the detection of CH_4 and CO_2 signals. Breakthrough curves of a mixture containing 5%CO_2 and 15%CH_4 in Helium were obtained passing the gas mixture on a cartridge filled with 109 g of carbon C. The sample was dried at 393 K for 2 h before the analysis. The experiment was performed at 298 K and 10 bar at a flowrate of 1200 ml/min in a mixSorb L (3P Instruments, Leipzig, Germany). The instrument used a TCD for the analysis of the gas mixture.

Static adsorption of hydrocarbons (methane, ethane, ethylene, propylene and propane) was evaluated via equilibrium adsorption.

Static adsorption experiments were performed in a home-built manometric equipment at 298 K with samples previously degassed at 523 K overnight. The instrument was designed and constructed by the LMA group and it's now licensed by Quantachrome Instruments as VStar (www.quantachrome.com).

Gas chromatographic separation of hydrocarbons was evaluated using the packed chromatographic columns described above, and 100 μl gas mix of ethane (1%), propylene (0.5%), propane (1%). Helium was used as the carrier gas (100 ml/min) and the gas signals were detected using a flame ionization detector (FID). The temperature of the oven was set at 308 K (1 min hold) then heated at 8 K/min to 513 K and hold for 30 min.

3. Results and discussion

3.1. Surface and elemental analysis of the synthesized carbon materials

The surface chemistry analysis of the carbon materials showed that the adsorbents contained oxygen in the surface which was in agreement with the oxygen content of mildly oxidized carbons [27]. The O(at%) and O/C wasn't significantly different among the four samples and it is not expected to play a role in their separation performance (Table 1). Consistent with the surface analysis, the elemental analysis values didn't show significant differences among the samples. The nitrogen values in the elemental analysis came from entrapped air in the carbon particles, and it was confirmed by the XPS analysis (Fig. 1.1) which didn't show nitrogen presence on the surface.

3.2. Immersion calorimetry measurements

In immersion calorimetry measurements, the enthalpy of adsorption would be larger for probe molecules that access the pores easily and lower for the opposite case. As it can be observed in Fig. 1.2, the accessibility for a small molecule such as dichloromethane (DCM-0.33 nm) is larger for sample D, followed by A, B and C, in agreement with the BET surface area. From the calorimetric data we estimated the surface area accessed by DCM (using a carbon black as a reference). S_{DCM} values were close to BET surface area values, except for samples with narrow micropores (e.g., C) where there was a larger deviation (Table 2). We believe S_{DCM} was more precise than S_{BET} because one monolayer of N_2 was formed in the porosity, with the corresponding underestimation in the case of the BET, while wetting of DCM took place in both sides of the pore. This difference became smaller for samples A and B due to the presence of slightly wider micropores able to accommodate up to two adsorbed layers (in this specific case $S_{DCM} \sim S_{BET}$). Conversely, the opposite extreme took place for sample D which had pores that fit three adsorbed layers; in this case, BET overestimated the surface area and $S_{DCM} < S_{BET}$. After DCM measurements, the enthalpy for a larger molecule such as 2-MP with 0.5 nm was measured. Because the 2-MP enthalpy values were close to that of DCM, there was indication that the porosity was wider than 0.5 nm (since both DCM and 2-MP were able to enter the porosity). Only in the case of sample C, the enthalpy for 2-MP was low, the open question was: Why a molecule with 0.5 nm was not able to access the porosity? were pores uniform and with a pore size less than 0.5 nm? to answer these questions for sample C, in a second step, we measured the enthalpy for an intermediate molecule, n-hx. If n-hx enthalpy had been similar to that of DCM, then we could have confirmed that the sample had uniform pores below 0.43 nm, i.e. pores where n-hx could enter but not 2-MP. However, calorimetry showed that also n-hx was partially excluded, thus confirming that part of the pores in sample C were larger than 0.43 nm and smaller than 0.5 nm. Finally, alpha-pinene with 0.7 nm was completely excluded from the porosity in sample C. Consequently, these results confirmed that sample C contained exclusively ultramicropores and that these micropores were in the 0.43–0.5 nm range. Note that calorimetry measurements were able to identify differences among the samples below 5 Å. Concerning sample B, the enthalpy of immersion also decreased with an increase in the kinetic diameter of the probe molecule although pores were slightly wider than C (in fact, 2-MP has a large accessibility and alpha-pinene do so). Calorimetry measurements showed that pores were wider for samples A and D since all molecules evaluated exhibited a significant accessibility. We then tried to measure the enthalpy for a molecule like 1,3,5-triisopropylbenzene with a diameter of 0.85 nm in samples A and D. Surprisingly, results were like those for alpha-pinene with a lower kinetic diameter (or even similar for sample B). Considering that 1,3,5-TIPB is a flat molecule (0.74 nm in width), the similarity with alpha-pinene gave an indication of the pore shape in these CMS; likely, these carbons had a slit-shape rather than a cylindrical shape allowing 1,3,5-TIPB and α-pinene similar accessibility.

3.3. N_2 adsorption data at 77 K

The textural properties of the Supelco® carbons were evaluated using nitrogen adsorption at 77 K. Isotherms in linear (Fig. 1.3) and logarithmic scale (Fig. 1.4) are shown for the four samples evaluated. As it can be observed in Fig. 1.3, sample D exhibited the largest adsorption capacity followed by samples A, B and finally C. Moreover, the knee of the nitrogen isotherm (see linear scale) at low relative pressures is narrower for sample C anticipating a narrow micropore size distribution, and it widens for the other samples with some development of mesoporosity (a hysteresis loop can be appreciated above $p/p_0 = 0.5$) preferentially for sample D. When plotted in logarithmic scale, (Fig. 1.4), all samples exhibited a similar adsorption profile at low relative pressures ($<10^{-4}$) except sample C with a higher adsorption capacity due to the presence of a stronger adsorption potential associated with the presence of narrower micropores; this observation suggested that microporosity in sample C was narrower compared to the other carbon samples. During N_2 adsorption data collection, the time needed at the manifold to reach equilibrium in each adsorption point was recorded. Although monitoring this time was not a standard kinetic analysis since gas doses were expanded into an already pressurized sample holder (from the previous isotherm dose), the evaluation of

Table 1
C, O and C/O concentration in the surface of the four carbons.

Sample	Elemental analysis (%)				Surface analysis (at%)		
	C	H	N	O	C	O	O/C
A	95.6 ± 0.1	0.74 ± 0.02	0.49 ± 0.07	3.2 ± 0.1	96.0 ± 0.4	3.4 ± 0.3	0.04 ± 0.01
B	95.5 ± 0.1	0.82 ± 0.01	0.47 ± 0.05	3.3 ± 0.1	96.9 ± 1.0	2.4 ± 0.4	0.02 ± 0.01
C	94.9 ± 0.2	0.87 ± 0.03	0.38 ± 0.04	3.9 ± 0.2	94.4 ± 1.7	3.0 ± 1.0	0.03 ± 0.01
D	95.2 ± 0.2	0.69 ± 0.03	0.43 ± 0.1	3.7 ± 0.3	97.1 ± 0.5	2.5 ± 0.2	0.03 ± 0.01

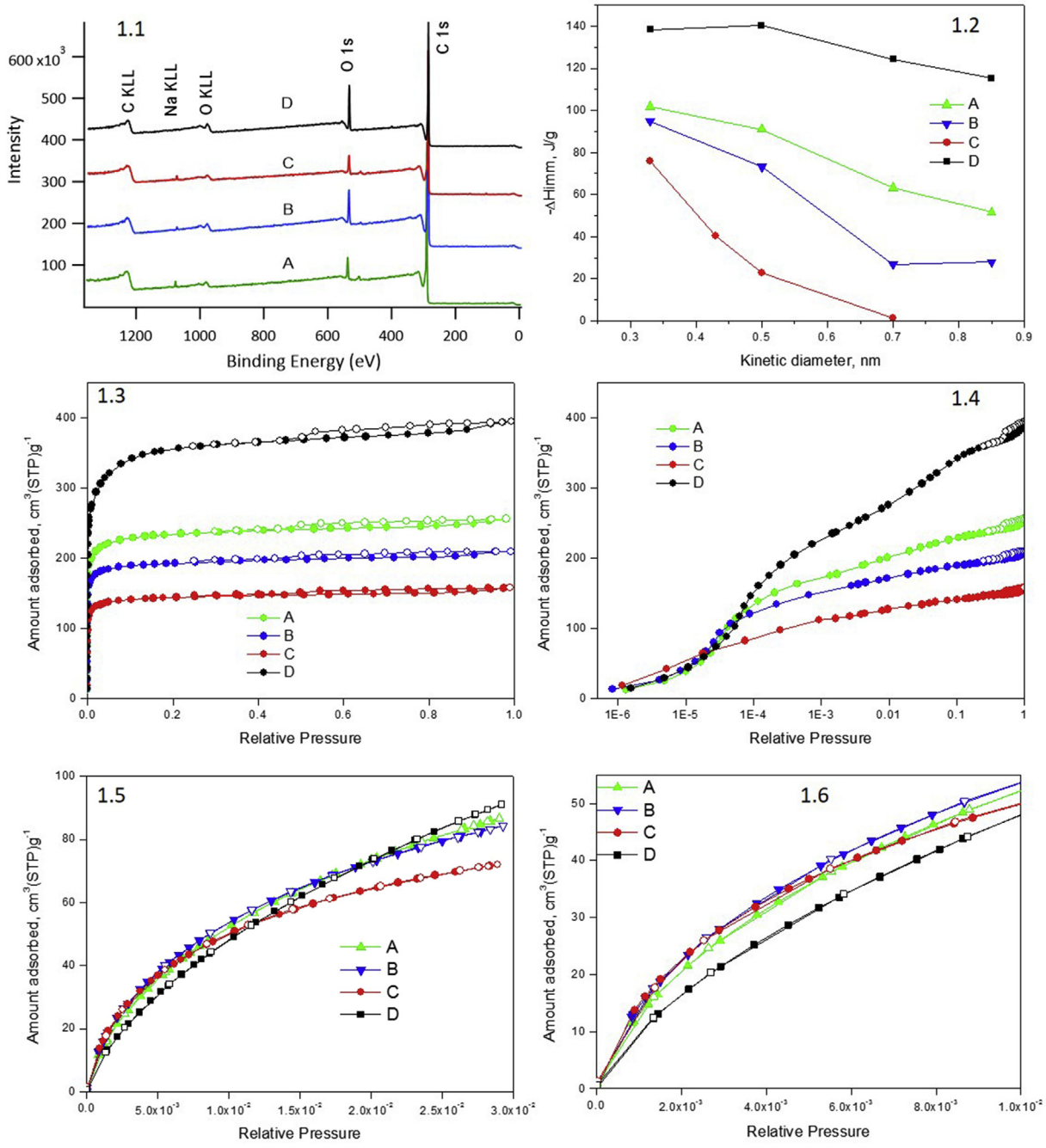

Fig. 1. XPS spectra (1.1). Pore size distribution obtained experimentally from enthalpy measurements at 303 K (1.2). High resolution N_2 adsorption isotherms at 77 K; linear scale (1.3), logarithmic scale (1.4). CO_2 adsorption isotherms at 273 K (1.5). CO_2 adsorption isotherm at 273 K at low pressures (1.6).

Table 2
Enthalpy of immersion into liquids of different dimensions.

Sample/Liquid	ΔH_{imm} (J/g)					S_{BET} (m^2/g)	S_{DCM} (m^2/g)	% deviation[a]
	DCM (0.33 nm)	n-hx (0.43 nm)	2-MP (0.5 nm)	α-pinene (0.7 nm)	1,3,5-TIPB (0.74 × 0.85 nm)			
A	−101.8	–	−91.0	−63.3	−51.7	902	983	9.0
B	−95.0	–	−73.2	−26.9	−27.9	762	843	10.6
C	−76.0	−41.6	−22.8	−1.4	–	558	674	20.8
D	−138.4	–	−140.3	−124.3	−115.3	1313	1228	−6.5

[a] Deviation between the surface area estimated from the N_2 adsorption data (after application of the BET equation) and the surface area estimated from dichloromethane (from the calorimetric measurements).

the time required to reach equilibrium provided insight about the presence of kinetically restricted constrictions in these samples. In the relative pressure range 10^{-6} up to 10^{-2} which corresponds to the filling of the narrow micropores, sample C required the longest time to reach equilibrium, followed by B with long equilibrium times in certain sections of the isotherm. On the other hand, the fact that for samples A and D, the different gas doses were equilibrated relatively fast indicated that A and D didn't exhibit kinetic limitations for N_2. Even though, the time taken for the manifold was not a true kinetic measurement, these observations highlighted the problems of nitrogen to access narrow porosity at low relative pressures. A summary of the equilibrium time in the relative pressure range from 10^{-6} up to 10^{-2} was illustrated in Fig. 2.

3.4. CO_2 adsorption isotherms at 273 K

The porosity of the carbon samples was also evaluated using CO_2 adsorption at 273 K. Under these conditions, CO_2 adsorption takes place up to 0.03 relative pressure, thus filling only the narrow micropores (those below 1 nm). Consequently, CO_2 adsorption complemented nitrogen adsorption in the evaluation of ultramicroporosity due to: i) the smaller size of the probe molecule (0.33 nm vs. 0.36 nm for N_2), and ii) the higher temperature of the measurement (273 K vs. 77 K). These two characteristics make CO_2 a suitable gas for samples where kinetic restrictions can be expected [13]. As it was observed in Fig. 1.5, CO_2 adsorption isotherms exhibited differences among the evaluated samples; the CO_2 adsorption isotherm in sample C exhibited a highly concave shape, thus denoting the presence of a strong adsorption potential, in close agreement with the nitrogen adsorption data described above. CO_2 adsorption in sample C exhibited a slightly higher adsorption capacity at low relative pressures (as in it can be seen in the zoom-in part of the isotherm Fig. 1.6). Samples C and B were slightly above sample A. Once narrow micropores were filled in sample C, the isotherm set on a plateau because wider micropores (0.7–1.0 nm) were not present. The adsorption isotherm of A, B, and D continuous to increase at mid pressures and exceeded that of C. Whereas, the total adsorption capacity was rather similar for samples A, B and D, the total capacity was the lowest for sample C. These observations agreed with the exclusive presence of ultramicroporosity in sample C. Concerning sample D, CO_2 adsorption results showed a lower concave shape, thus anticipating the presence of a wider pore size distribution in this sample and the weaker adsorption potential for CO_2 at low relative pressures. Sample D also exhibited the largest BET surface area, followed by A, B and finally C. The surface area and total micropore volumes trends agreed with the assumption that N_2 adsorption estimated the total micropore volume while CO_2 only provided the narrow micropore volume (<1 nm). With CO_2 data, the Dubinin-Radushkevich equation was applied to estimate narrow micropore volume (Table 3). For sample C, the CO_2 volume was larger than the N_2 volume showing that C was a carbon molecular sieve with accessibility limitations for N_2 at 77 K. Some micropores in this sample were inaccessible to N_2, in agreement with the larger equilibration times

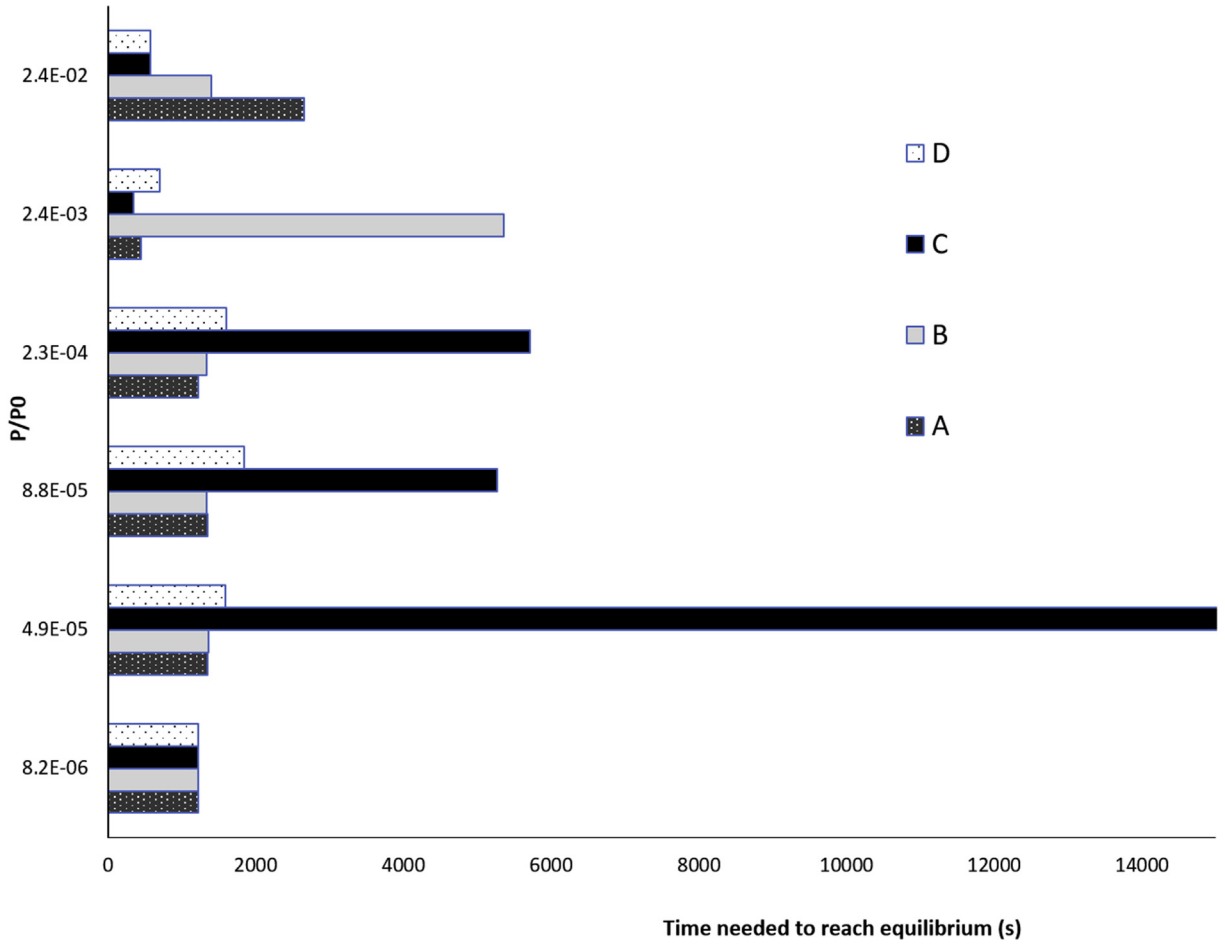

Fig. 2. Time required at the manifold to reach equilibrium for each individual point in the nitrogen adsorption isotherm.

Table 3
Total micropore volume, ultra and supermicropore volume obtained from the N2, O2 and Ar adsorption and calculated 2D-NLDFT models. CO2 Narrow micropore volume was obtained after application of the DR equation.

Sample	SBET (m^2/g)	Total micropore volume (cm3/g)				Ultramicropore volume (cm^3/g)			Supermicropore volume (cm^3/g)		
		O_2	Ar	N_2	CO_2	O_2	Ar	N_2	O_2	Ar	N_2
A	902	0.39	0.37	0.38	0.33	0.25	0.23	0.26	0.15	0.13	0.12
B	762	0.32	0.28	0.29	0.30	0.25	0.21	0.25	0.07	0.07	0.05
C	558	0.22	0.20	0.21	0.24	0.20	0.16	0.18	0.02	0.04	0.03
D	1313	0.55	0.55	0.51	0.40	0.22	0.23	0.24	0.33	0.32	0.27

described in Fig. 2. In sample B, the similarity between both pore volumes (0.29 cm^3/g for both N_2 and 0.30 cm^3/g for CO_2 adsorption) anticipated that sample B was also a carbon molecular sieve with narrow micropores (although exhibited less kinetic restrictions for N_2 accessibility at 77 K than carbon C); both N_2 and CO_2 filled a similar porosity. Meanwhile, samples A and D didn't exhibit any kinetic limitation and the larger volume for N_2 versus CO_2 anticipated a wider pore size distribution. Although, CO_2 measurements didn't account for the pore volume in pores larger than 1 nm; samples A and D contained a larger proportion of pores above 1 nm, as it was confirmed using 2D-NLDFT calculations (Table 3).

3.5. Ar and O_2 adsorption isotherms at cryogenic temperatures

To confirm the textural properties observed with immersion calorimetry, and N_2 and CO_2 adsorption, Ar and O_2 isotherms were measured at 87 K and 77 K, respectively. The pore size distributions for the CMS were calculated from N_2, Ar and O_2 isotherms using recently developed 2D-NLDFT models [12]. Fits of the corresponding models for all N_2, Ar and O_2 data using SAIEUS software [28] were plotted in Fig. 3. The PSDs calculated from N_2, Ar and O_2 exhibited similar values for all samples in terms of differential (Fig. 4) and cumulative (Fig. 5) PSDs. The 2D-NLDFT calculations showed, using models for N_2, Ar and O_2, that all the carbons were microporous only and that sample C had the narrowest pore size distribution followed by B, A and D, respectively. The PSD suggested that sample C possessed ultramicropores only (below 7 Å), whereas the other samples had pores above 7 Å; this result was in agreement with the calorimetric data. Based on both theoretical predictions and calorimetric data, the PSD above 0.7 nm widens from

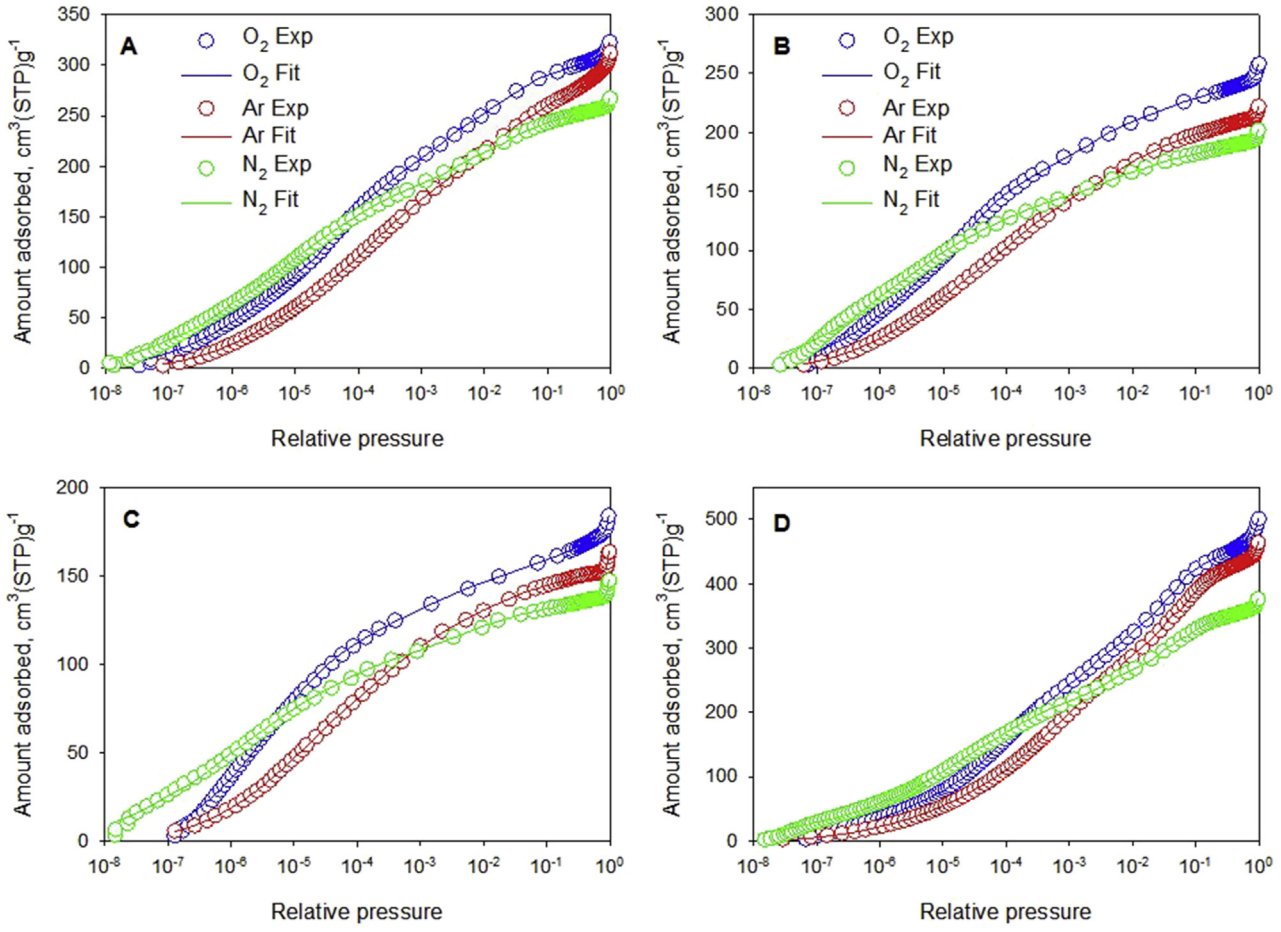

Fig. 3. Experimental adsorption isotherms of argon at 87 K, oxygen and nitrogen at 77 K measured for all four samples are shown as circles. Fits of the 2D-NLDFT models to the data are shown as continuous lines.

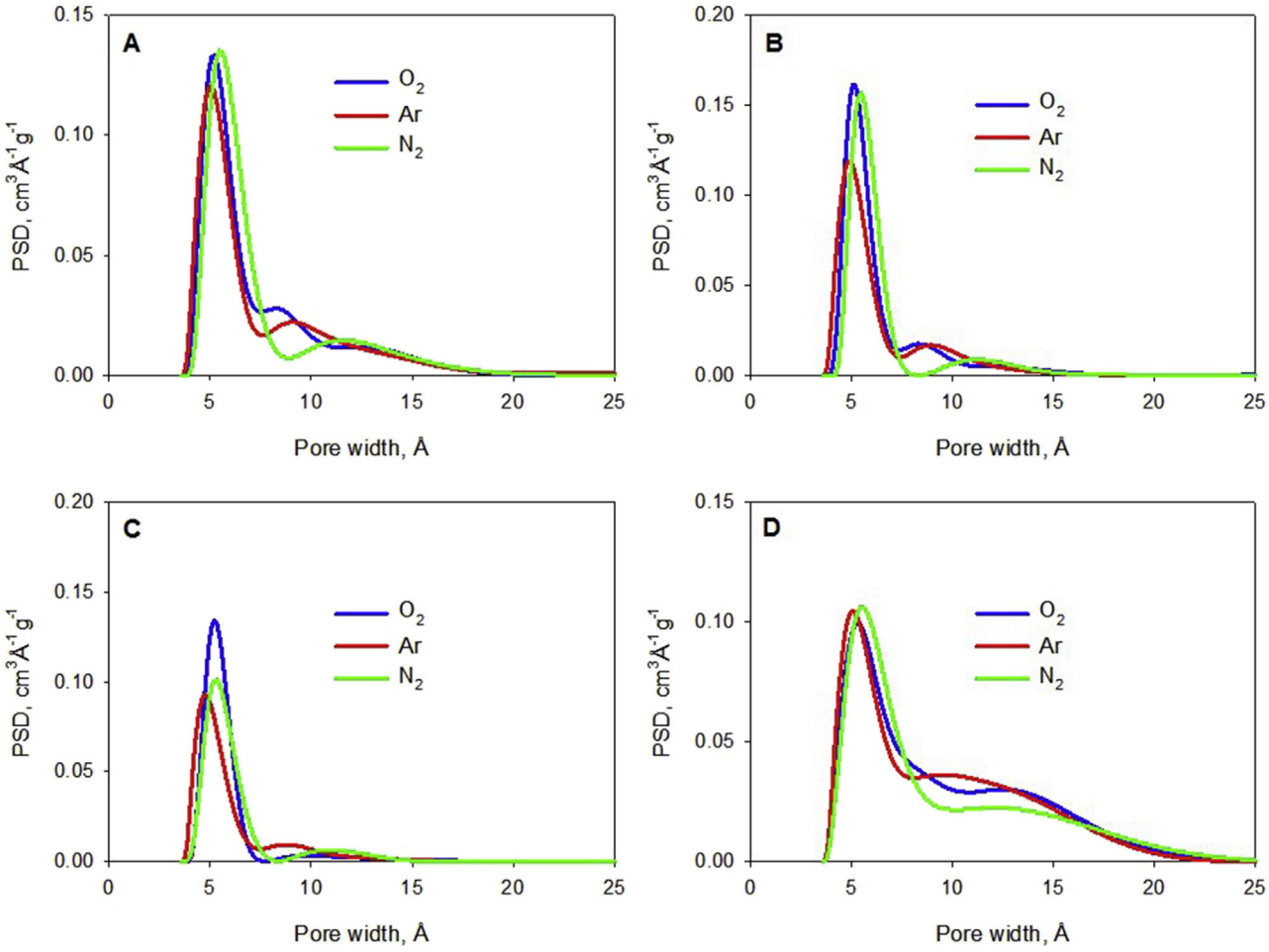

Fig. 4. Differential pore size distributions calculated from the adsorption isotherms of argon at 87 K, oxygen and nitrogen at 77 K for samples A, B, C, and D.

sample B to A and D. The PSD for sample D showed a larger development of supermicropores, the presence of supermicroporosity in sample D explained the smaller CO_2 capacity at low relative pressures.

The micropore volume was obtained from the adsorption data for all probes used, O_2, Ar, N_2 and CO_2 (Table 3). According to the IUPAC classification, the total micropore volume was the volume of gas adsorbed below 20 Å [11]. The ultramicropore volume is the volume gas adsorbed below 7 Å while the supermicropore volume is that between 7 and 20 Å[29]. The results obtained with O_2, Ar and N_2 probes were similar and showed the same trends for all carbons; the total micropore volume was larger for sample D, and was followed by A, B and C as also illustrated by Fig. 5. Carbons A, B, and D (0.25, 0.24, 0.23 ± 0.02) showed similar volumes of ultramicroporosity followed by samples C (0.18 ± 0.01). The larger differences among the carbons were observed in the supermicroporous region. The three probes O_2, Ar, N_2 predicted the absence of pores between 7 and 20 Å for sample C (0.03 ± 0.01) followed by sample B (0.06 ± 0.02). Sample B and C had most of the available micropore volume in the ultramicroporous region <7 Å, while those of samples A, and D showed a larger proportion of supermicropores (7–20 Å). Micropore volume data showed that O_2, N_2, and Ar molecules predicted the lowest supermicropore volume for sample C. Sample C was the only carbon of the series that was exclusively ultramicroporous.

3.6. Potential application of the synthesized carbon materials

3.6.1. High-pressure CH_4 and CO_2 isotherms at 298 K and dynamic tests

The equilibrium adsorption of these carbon materials was complemented with measurements of high-pressure adsorption. Isotherms for carbon dioxide and methane at 298 K at high pressure (up to 30 bar) showed the same trend observed in the textural characteristics (Fig. 6.1 and Fig. 6.2). Samples A and D have a larger capacity for CO_2 and CH_4 compared to samples B and C that became saturated at mid pressures. The ratio of CO_2 uptake with respect to CH_4 at 30 bar was calculated in molar basis as 1.57 for sample A, 1.44 for sample B, 1.38 for sample C and 1.65 for sample D. According to these uptake results, samples A (1.57) and D (1.65) which had larger pores and larger surface areas were better candidates for preferential adsorption of CO_2 over CH_4. The larger capacity of the carbons with wider porosity seemed to contradict reported results shown for porous carbons where carbons with larger ultramicropore volume adsorbed more CO_2 molecules than carbons with lower ultramicropore volume [30–32]. In this work, all carbons tested had both similar ultramicropore volumes ($0.20–0.25 \pm 0.02$ cm^3/g) and surface chemistry; therefore, the differences in CO_2 adsorption capacity were most probably due to the higher packing of CO_2 molecules compared to CH_4 in larger micropores compared to samples with smaller micropores where

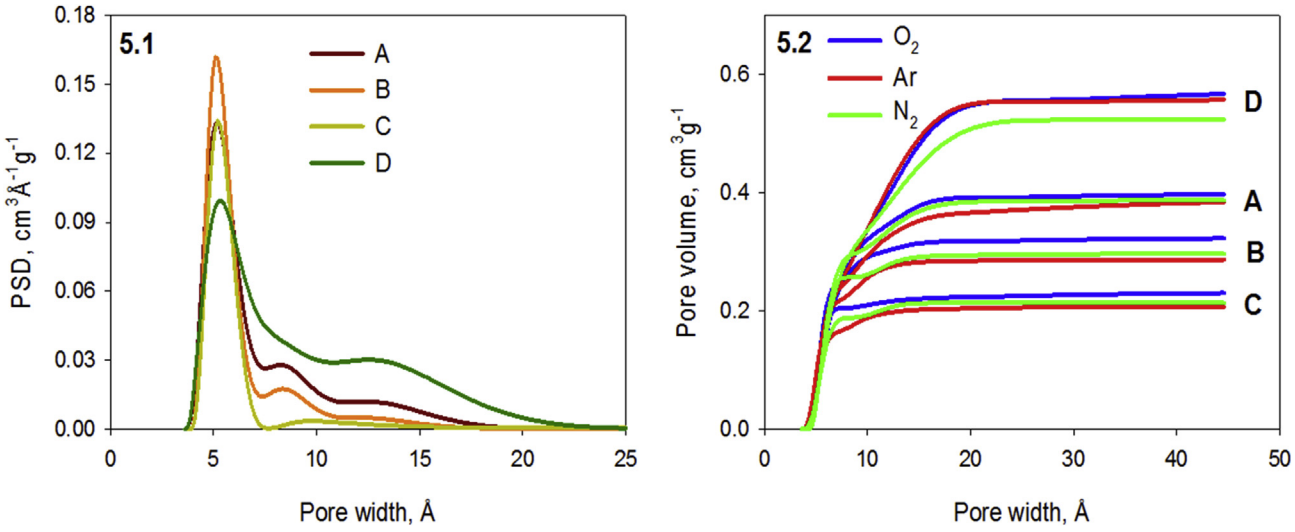

Fig. 5. Comparison between pore structures of studied carbon samples; PSDs calculated from oxygen at 77 K (5.1), cumulative pore size distributions calculated from Ar, O_2, and N_2 (5.2).

only a single layer could be adsorbed. On the contrary to the equilibrium adsorption results, the retention times for CO_2 followed the pore size distribution order; the dynamic test using gas chromatography experiments showed that carbon C having only ultramicropores retained CO_2 longer (85 min) than the carbons with developed supermicroporosity: carbon B (73 min), C (56 min) and D (30 min) (Table 4). A plot correlating, supermicroporous volume with respect to the difference in retention time was depicted in Fig.6.3. Even though, carbon D had larger capacity for CO_2 adsorption and larger volume of supermicropores, it was the absence of wider microporosity in carbon C that allowed it to adsorb CO_2 longer than CH_4 in dynamic conditions. The presence of supermicropores in carbon D explained why the retention time for CO_2 in carbon D was 55 min shorter than for carbon C. In carbon D, these wider micropores permitted CO_2 molecules to go in and out the pores faster than in Carbon C. The chromatographic separations of CH_4 and CO_2 were sensitive to pore size of the adsorbent; therefore, performance differences were evident among similar adsorbents. Consequently, the chromatographic test also gave information on the pore size distribution of carbon adsorbents. In this case, the performance of carbon C for the separation of CO_2/CH_4 indicated a smaller pore size distribution than the rest of carbons A, B, and D. Although pore size distributions measured and calculated by static systems showed small texture differences among the carbons evaluated, the pore size differences were enhanced when the carbons were tested in packed beds. O_2 adsorption at 77 K gave the lowest value of supermicroporosity for carbon C compared to N_2 or Ar.; although the difference was not significant, the supermicroporosity values indicated that O_2 might have given a more accurate evaluation of carbon materials with similar textural properties. Adsorption in the microporous region occurred due to enhanced interactions of the gas and solid phases [29]. Presence of mineral matter on an adsorbent could cause unwanted interactions of a gas probe such as O_2 with the solid. Consequently, care must be taken in the evaluation of samples containing inorganic contaminants (large ash content), since the presence of specific interactions of the O_2 molecule with metals can give rise to erroneous interpretations.

In agreement with the chromatographic results, the breakthrough curves for a CH_4 and CO_2 (Fig. 6.4) showed a rapid (15 min) breakthrough of CH_4 through the carbon column packed with carbon C while it took the CO_2 molecules 40 min to pass through. The separation of CO_2 and CH_4 yielded a "rollover effect" for methane; meaning that it seemed it was a larger volume fraction of CH_4 at the outlet compared to the inlet. The reason for this rollover effect was 5%CO_2 missing in the gas outlet during the overshoot period. Another reason for the rollover effect was displacement of adsorbed CH_4 with preferentially adsorbed CO_2; the desorbed CH_4 also contributed to the seemingly higher CH_4 concentration. The selectivity for CO_2 was calculated as 3.67 for a flow rate of 1200 ml/min, thus indicating ability of the ultramicroporous carbon C to separate CH_4 and CO_2. According to this elution order, in a pressure adsorption system CO_2 would be adsorbed (heavy component) while CH_4 would be recovered as the non-adsorbed (light) component.

3.6.2. Hydrocarbon adsorption and dynamic separation in activated carbons C & B

Carbon molecular sieves C & D were also evaluated for static adsorption of hydrocarbons (see Fig. 6.5 for data in sample C). The adsorption capacity for light hydrocarbons increased with the vapor pressure of the adsorbate molecule, going from a slightly concave performance for highly volatile methane to a type I isotherm for condensable C_3 isomers. Only sample C, with a smaller pore size distribution showed potential for equilibrium separation of the propane and propylene pair. Carbon C had larger equilibrium adsorption capacity for propylene compared to propane, which agreed with studies that showed propylene was preferentially adsorbed compare to propane on another CMS [33]. On the contrary, carbon D with wider micropores showed similar equilibrium capacity for ethane/ethylene and propane/propylene. Table 5 contains a summary of the data obtained for the different hydrocarbons under equilibrium conditions for both samples (C & D). As described above, selectivity to the unsaturated hydrocarbons (C_2H_4/C_2H_6 & C_3H_6/C_3H_8) was close to 1 for a carbon material with a wide micropore size distribution (i.e., sample D), whereas the exclusive presence of narrow constrictions (i.e., sample C) favored the propylene/propane separation with an increase in the selectivity up to 1.3. However, when tested in a dynamic mode using gas chromatography, the pair propane and propylene couldn't be resolved using carbon C and left the column as a single peak. Propane and propylene had difficulties entering the ultramicropores in

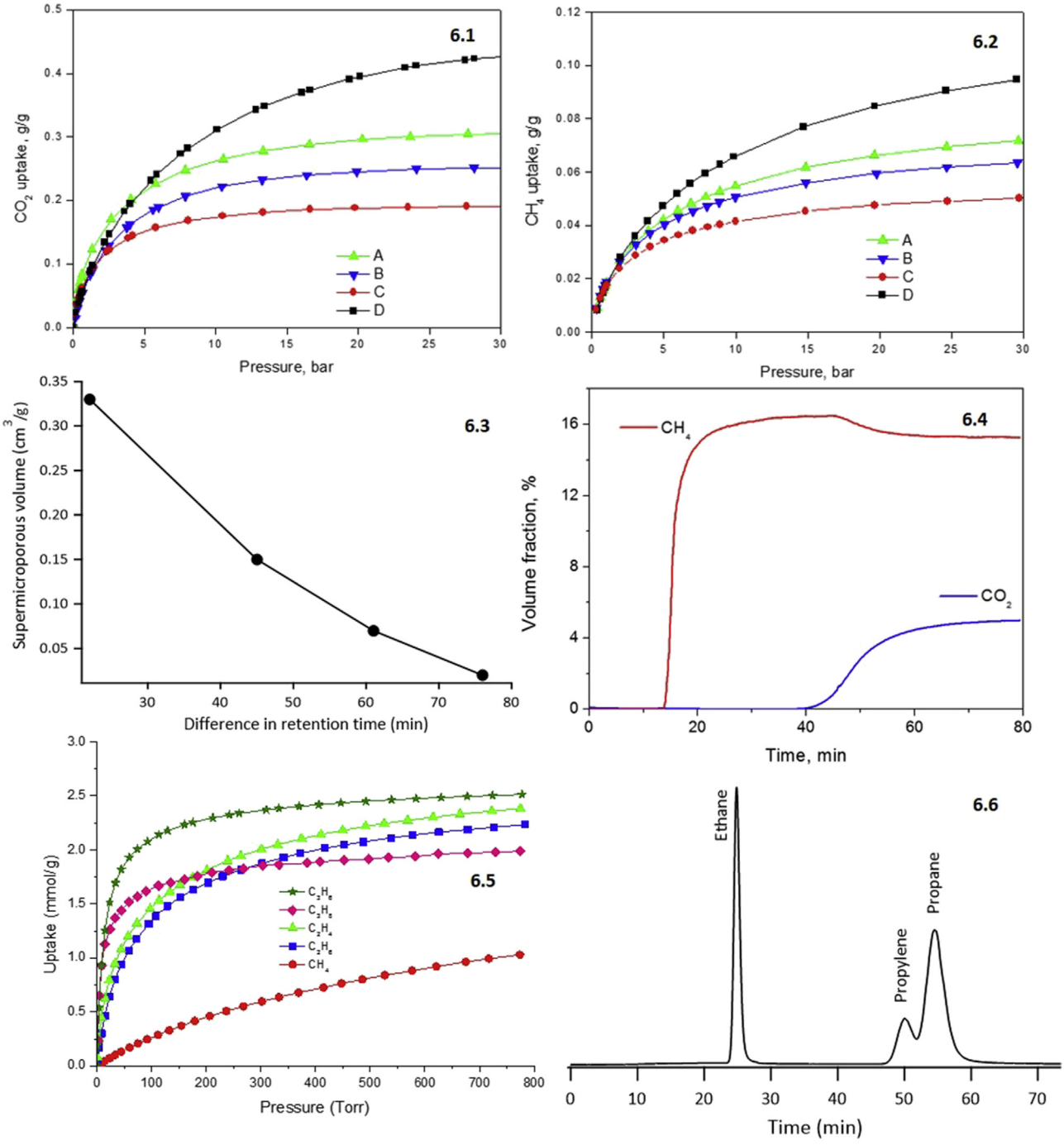

Fig. 6. High pressure adsorption isotherms for CO_2 (6.1) and CH_4 (6.2), the isotherms were measured at 298 K using pure gas; isotherms with square markers correspond to sample D, circles to A, triangles to B, and diamonds to C. Correlation of supermicroporous volume and retention time of CO_2 (6.3). CO_2 and CH_4 breakthrough curves at 1 MPa and 298 K on a column packed with carbon C (6.4). Adsorption of hydrocarbons at 298 K methane (circles), ethane (squares), ethylene (triangles), propane (diamonds), and propylene (stars) using Carbon C (6.5). Chromatographic separation of a gas mix containing ethane (1%), propylene (0.5%), propane (1%) using carbon D (6.6).

Table 4
Equilibrium (298 K, 30 bar) and Kinetic adsorption of CO_2 and CH_4 (308 K, 1 bar).

Sample	Amount adsorbed		Static	Dynamic	Retention time	
	CO_2 (mmol/g)	CH_4 (mmol/g)	$S_{CO2/CH4}$	$S_{CO2/CH4}$	CO_2 (min)	CH_4 (min)
C	4.31	3.12	1.38	3.67	85	9
B	5.70	3.96	1.44	-[a]	73	12
A	7.04	4.47	1.57	-[a]	56	11
D	9.77	5.90	1.65	-[a]	30	8

[a] Breakthrough curves were measured only for carbon C.

Table 5
Adsorption capacity at equilibrium for ethane, ethylene, propane and propylene, selectivity C2H4/C2H6 and C3H6/C3H8 at atmospheric pressure under equilibrium conditions and gas chromatography retention times.

Sample	Amount adsorbed (mmol/g)				Selectivity		Retention time (min)	
	C_2H_6	C_2H_4	C_3H_8	C_3H_6	$S_{C2H4/C2H6}$	$S_{C3H6/C3H8}$	C_3H_6	C_3H_8
C	2.23	2.38	1.98	2.51	1.07	1.27	40.3	40.3
D	5.46	5.69	4.06	3.75	1.04	0.92	50.6	54.6

carbon C under dynamic conditions; both molecules broke through the column simultaneously. Shorter retention times in carbon C indicated that the ultramicropores were not utilized by the gas molecules; the molecules bypassed the narrow pores and spent more time in the interstitial space of the packed bed. Conversely, Carbon D which contained both ultramicropores and supermicropores separated the propane/propylene pair. The presence of supermicropores promoted the access of gas molecules into the ultramicropores. The propylene molecules moved quicker in and out of the micropores compared to propane molecules which allowed separation of the pair. Moreover, a longer retention time (50.6 min) in carbon D compared to 40.3 min retention time for Carbon C evidenced the utilization of the ultramicropores by the gas molecules. As expected in chromatography profiles [34], propylene eluted earlier than propane since small size molecules (propylene 4.0 Å) eluted faster than larger molecules (propane 4.3 Å) (Fig. 6.6). Similar results were reported in packed bed experiments which showed propane broke through the column later than propylene in another CMS and it was explained by the slower diffusion of propane in small pores [25]. At high concentrations such those used for PSA systems, the propylene was adsorbed in the pores and therefore retained longer, in this case, propylene was the heavy compound and it was recovered during the desorption step [8].

4. Conclusions

The combination of gas adsorption with immersion calorimetry into liquids of different kinetic diameter allowed the evaluation of textural properties (pore size distribution and pore shape) in carbon materials. The pore size distributions from theoretical 2D-NLDFT models using O_2 Ar and N_2 as probe molecules agreed with the results from immersion calorimetry. PSD profiles obtained using O_2, Ar and N_2 isotherms were similar and showed the same trends for the four CMS analyzed. O_2 probe demonstrated textural differences among molecular sieves with similar textural porosity. The theoretical calculations as well as the calorimetry tests showed that sample C had the narrowest pore size distribution followed by B, A and D, respectively. PSD revealed that sample C was microporous with most of the available volume in the ultramicroporous region, while samples B, A, and D exhibited a larger fraction of supermicropores. The textural properties of the carbons helped to explain the performance of these carbons during gas separation studies. For separation of CO_2 and CH_4 at pressure, carbons A and D, which had supermicropores, showed an increased equilibrium adsorption capacity for CO_2 and CH_4 at 30 bar compared to carbons B and C which contained mostly ultramicropores; However, sample C with narrow pores showed longer retention times for CO_2 in gas chromatographic experiments at 0.3 bar. The kinetic selectivity of carbon C for CO_2 vs. CH_4 was also estimated as 3.67 and indicated ability of the ultramicroporous only carbon to separate CH_4 and CO_2 in a continuously fed column. For the separation of small hydrocarbons, even though sample C showed larger equilibrium capacity for propylene vs. propane, carbon D containing supermicroporous achieved the separation of propane and propylene from a hydrocarbon mixture under dynamic conditions.

Declaration of competing interest

The authors declare that they have no known competing financial interests or personal relationships that could have appeared to influence the work reported in this paper.

Acknowledgments

The authors would like to thank Robert Eschrich from 3P-Instruments for his help with the breakthrough analysis. We would also like to thank Jeffrey Schallenberg from the Materials Characterization Lab at The Pennsylvania State University for his help with the XPS analysis. JSA would like to acknowledge financial support from the Ministerio de Economía y Competitividad (MINECO) (MAT2016-80285-p), Generalitat Valenciana (PROMETEOII/2014/004) and H2020 (MSCA-RISE-2016/NanoMed Project).

References

[1] Y. Yang, N. Burke, A. Suhaib, S. Huang, S. Li, Y. Zhou, et al., Experimental studies of hydrocarbon separation on zeolites, activated carbons and MOFs for applications in natural gas processing, RSC Adv. 7 (2017) 12629–12638.
[2] L. Pereira, Porous graphitic carbon as a stationary phase in HPLC: theory and applications, J. Liq. Chromatogr. Relat. Technol. 31 (2008) 1687–1731.
[3] A. Kapoor, R.T. Yang, Kinetic separation of methane-carbon dioxide mixture by adsorption on molecular sieve carbon, Chem. Eng. Sci. 44 (1989) 1723–1733.
[4] Y. Li, D. Li, Y. Rao, X. Zhao, M. Wu, Superior CO2, CH4, and H2 uptakes over ultrahigh-surface-area carbon spheres prepared from sustainable biomass-derived char by CO2 activation, Carbon N. Y. 105 (2016) 454–462.
[5] R. Augelletti, M. Conti, M.C. Annesini, Pressure swing adsorption for biogas upgrading. A new process configuration for the separation of biomethane and carbon dioxide, J. Clean. Prod. 140 (2017) 1390–1398.
[6] R.L. Siegelman, P.J. Milner, E.J. Kim, S.C. Weston, J.R. Long, Challenges and opportunities for adsorption-based CO 2 capture from natural gas combined cycle emissions, Energy Environ. Sci. 12 (2019) 2161–2173.
[7] D.S. Sholl, R.P. Lively, Seven chemical separations to change the world, Nature 532 (2016) 6–9.
[8] C.A. Grande, S. Cavenati, F.A. Da Silva, A.E. Rodrigues, Carbon molecular sieves for hydrocarbon separations by adsorption, Ind. Eng. Chem. Res. 44 (2005) 7218–7227.
[9] C.A. Grande, V.M.T.M. Silva, C. Gigola, A.E. Rodrigues, Adsorption of propane and propylene onto carbon molecular sieve, Carbon N. Y. 41 (2003) 2533–2545.
[10] J. Silvestre-Albero, A. Silvestre-Albero, F. Rodríguez-Reinoso, M. Thommes, Physical characterization of activated carbons with narrow microporosity by nitrogen (77.4 K), carbon dioxide (273 K) and argon (87.3 K) adsorption in combination with immersion calorimetry, Carbon N. Y. 50 (2012) 3128–3133.
[11] M. Thommes, K. Kaneko, A.V. Neimark, J.P. Olivier, F. Rodríguez-Reinoso, J. Rouquerol, et al., Physisorption of gases, with special reference to the evaluation of surface area and pore size distribution (IUPAC Technical Report), Pure Appl. Chem. 87 (2015) 1051–1069.
[12] J. Jagiello, J. Kenvin, Consistency of carbon nanopore characteristics derived from adsorption of simple gases and 2D-NLDFT models. Advantages of using adsorption isotherms of oxygen (O 2) at 77 K, J. Colloid Interface Sci. 542 (2019) 151–158.
[13] F. Rodríguez-Reinoso, J. Garrido, J.M. Martín-Martínez, M. Molina-Sabio, R. Torregrosa, The combined use of different approaches in the characterization of microporous carbons, Carbon 27 (1989) 23–32.
[14] R.V.R.A. Rios, A. Sepúlveda-Escribano, M. Molina-sabio, F. Rodríguez-Reinoso, Kinetic restrictions in the characterization of narrow microporosity in carbon materials, J. Phys. Chem. Lett., 2007, pp. 3803–3805.
[15] J. Jagiello, W. Betz, Characterization of pore structure of carbon molecular sieves using DFT analysis of Ar and H2adsorption data, Microp. Mesop. Mater. 108 (2008) 117–122.
[16] J. Jagiello, C. Ania, J.B. Parra, C. Cook, Dual gas analysis of microporous carbons using 2D-NLDFT heterogeneous surface model and combined adsorption data of N2 and CO2, Carbon N. Y. 91 (2015) 330–337.
[17] J. Jagiello, J.P. Olivier, 2D-NLDFT adsorption models for carbon slit-shaped pores with surface energetical heterogeneity and geometrical corrugation, Carbon N. Y. 55 (2013) 70–80.
[18] J. Silvestre-Albero, C. Gómez de Salazar, A. Sepúlveda-Escribano, F. Rodríguez-Reinoso, Characterization of microporous solids by immersion calorimetry, Colloid. Surf. Physicochem. Eng. Asp. 187 (2001) 151–165.
[19] D.P. Broom, K.M. Thomas, Gas adsorption by nanoporous materials: future

applications and experimental challenges, MRS Bull. 38 (2013) 412–421.
[20] D.P. Broom, Characterizing adsorbents for gas separations, Chem. Eng. Prog. 114 (2018) 30–37.
[21] M. Thommes, C. Morlay, R. Ahmad, J.P. Joly, Assessing surface chemistry and pore structure of active carbons by a combination of physisorption (H2O, Ar, N2, CO2), XPS and TPD-MS, Adsorption 17 (2011) 653–661.
[22] S.K. Bhatia, Density functional theory analysis of the influence of pore wall heterogeneity on adsorption in carbons, Langmuir 18 (2002) 6845–6856.
[23] D.D. Do, H.D. Do, Modeling of adsorption on nongraphitized carbon surface: GCMC simulation studies and comparison with experimental data, J. Phys. Chem. B 110 (2006) 17531–17538.
[24] S. Sircar, J.R. Hufton, Why does the linear driving force model for adsorption kinetics work? Adsorption 6 (2000) 137–147.
[25] J. Liu, Y. Liu, T. Kayrak, E. Calverley, M. Brayden, M. Martinez, et al., A new carbon molecular sieve for propylene/propane separations, Carbon N. Y. 85 (2015) 201–211.
[26] A.M. Silvestre-Albero, A. Wahby, J. Silvestre-Albero, F. Rodríguez-Reinoso, W. Betz, Carbon molecular sieves prepared from polymeric precursors: porous structure and hydrogen adsorption properties, Ind. Eng. Chem. Res. 48 (2009) 7125–7131.
[27] J.L. Figuereido, M.F.R. Pereira, M.M.A. Freitas, J.J.M. Orfao, Modification of the surface chemistry of activated carbons, Carbon N. Y. 37 (1999) 1379–1389.
[28] J. Jagiełło, Stable numerical solution of the adsorption integral equation using splines, Langmuir 10 (1994) 2778–2785.
[29] P.J.M. Carrott, R.A. Roberts, K.S.W. Sing, Adsorption of nitrogen by porous and non-porous carbons, Carbon N. Y. 25 (1987) 59–68.
[30] Z. Zhang, D. Lou, G. Lui, G. Li, G. Jiang, Z.P. Cano, et al., In-situ ion-activated carbon nanospheres with tunable ultramicroporosity for superior CO2 capture, Carbon 143 (2019) 531–541.
[31] V. Presser, J. Mcdonough, S. Yeon, Y. Gogotsi, Effect of pore size on carbon dioxide sorption by carbide derived carbon, Energy Environ. Sci. 4 (2011) 3059–3066.
[32] J. Zhou, Z. Li, W. Xing, H. Shen, X. Bi, T. Zhu, et al., A New Approach to Tuning Carbon Ultramicropore Size at Sub-angstrom Level for Maximizing Specific Capacitance and CO 2 Uptake, Adv. Funct. Mater., 2016, pp. 7955–7964.
[33] C.A. Grande, A.E. Rodrigues, Adsorption of binary mixtures of Propane–Propylene in carbon molecular sieve 4A, Ind. Eng. Chem. Res. 43 (2004) 8057–8065.
[34] W.R. Betz, S.J. Lambiase, Dynamic gas solid chromatographic techniques for characterizing carbon molecular-sieves, J. Chromatogr. 556 (1991) 433–440.